Tomographic Dynamics and Scale-Dependent Viscosity in 2D Electron Systems

Patrick Ledwith,[1] Haoyu Guo,[1] Andrey Shytov,[2] and Leonid Levitov[1]

[1]*Massachusetts Institute of Technology, Cambridge, Massachusetts 02139, USA*
[2]*School of Physics, University of Exeter, Stocker Road, Exeter EX4 4QL, United Kingdom*

Fermi gases in two dimensions display collective dynamics originating from head-on collisions, a collinear carrier scattering process that dominates angular relaxation at not-too-high temperatures $T \ll T_F$. In this regime, a large family of excitations emerges, with an odd-parity angular structure of momentum distribution and exceptionally long lifetimes. This leads to "tomographic" dynamics: fast 1D spatial diffusion along the unchanging velocity direction accompanied by a slow angular dynamics that gradually randomizes velocity orientation. The tomographic regime features an unusual hierarchy of timescales and scale-dependent transport coefficients with nontrivial fractional scaling dimensions, leading to fractional-power current flow profiles and unusual conductance scaling versus sample width.

Disorder-free electron systems in which the electron-electron (*ee*) collisions are predominantly momentum conserving can exhibit a hydrodynamic behavior reminiscent of that in viscous fluids [1–5]. Electron hydrodynamics, a theoretical concept describing this regime in terms of quasiparticle scattering near the Fermi surface, has been steadily gaining support in recent years for a range of electronic systems [6–22]. On the experimental front, many hydrodynamic signatures have been observed in graphene, both in the Dirac fluid at charge neutrality [23] and in the Fermi liquid state created by doping away from charge neutrality [24–27].

Given that two-dimensional (2D) Fermi liquids are at the focus of current experimental efforts [24–29], it is timely to revisit theoretical foundations of electron hydrodynamics of these systems. Here we argue that our theoretical understanding is thoroughly incomplete and is in need of revision. Indeed, it is usually taken for granted that hydrodynamics in 2D Fermi liquids sets in at the length scales $r > l_{ee} = v/\gamma$, where $\gamma \sim T^2/T_F$ is the *ee* collision rate and v is the Fermi velocity. However, generic large-angle quasiparticle scattering at a thermally broadened 2D Fermi surface is known to be inhibited by fermion exclusion, except for the head-on scattering processes [30–32]. As discussed below, the head-on collisions completely reshape electron hydrodynamics, creating new dynamical regimes and new length scales.

Indeed, as illustrated in Fig. 1, because of the joint effect of the kinematic constraints and fermion exclusion, it is the head-on collisions that dominate angular relaxation at a 2D Fermi surface. These processes do lead to rapid momentum exchange between particles, however with one caveat: head-on collisions change particle distribution in an identical way simultaneously at momenta **p** and −**p**, providing a relaxation pathway only for the part of the momentum

distribution which is *even* under Fermi surface inversion, $\delta f_{-\mathbf{p}} = \delta f_{\mathbf{p}}$. The odd-parity part, $\delta f_{-\mathbf{p}} = -\delta f_{\mathbf{p}}$, does not relax due to such processes, giving rise to a large number of soft modes [20,33]. This peculiar behavior is generic in 2D Fermi liquids at $T \ll T_F$, so long as the *ee* collisions are momentum conserving.

The new regime, dominated by the head-on collisions and odd-parity harmonics, occurs at the length scales (and frequencies) in between the conventional ballistic and hydrodynamic regimes,

$$l_{ee} < r < \xi = \frac{v}{\sqrt{\gamma' \gamma}}, \tag{1}$$

where $\xi \gg l_{ee}$ is a new length scale originating from slowly relaxing odd-parity modes. Here the rate $\gamma \sim T^2/T_F$ describes head-on processes and even-parity modes, the
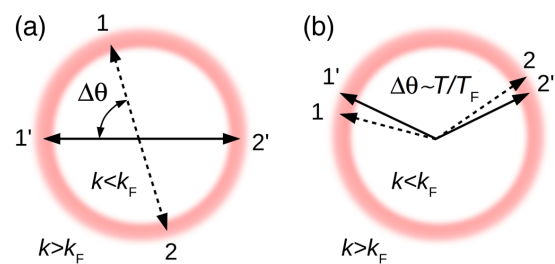

FIG. 1. Types of two-body collisions $1, 2 \to 1', 2'$ at a thermally broadened 2D Fermi surface (red rings), which are allowed by momentum and energy conservation and not inhibited by fermion exclusion. Head-on collisions (a) occur at a rate $\gamma \sim T^2/T_F$, with typical recoil $\Delta\theta \sim 1$. Such processes, however, affect only the even-parity part of momentum distribution. The odd-parity part relaxes much slower, at a rate $\gamma' \sim T^4/T_F^3 \ll \gamma$ [33] due to processes illustrated in (b) and other non-head-on processes.

rate $\gamma' \ll \gamma$ describes slow odd-parity modes. The intrinsic γ' values due to small-angle ee scattering are estimated to be as low as [33]

$$\gamma' \sim (T/T_F)^2 \gamma \ll \gamma. \tag{2}$$

The conventional ballistic and hydrodynamic regimes occur at $r < l_{ee}$ and $r > \xi \gg l_{ee}$, respectively. In the ballistic regime the system features a standard free-particle behavior. Likewise, in the hydrodynamic regime transport coefficients assume their conventional values, e.g., the standard result $\nu = v^2/4\gamma$ for kinematic viscosity. However, at the intermediate scales Eq. (1) transport coefficients acquire a dependence on the wave number, becoming scale dependent with nontrivial scaling dimensions.

At this point one may ask whether these results contradict the many-body calculations predicting quasiparticle lifetimes scaling as $(1/\tau) \sim T^2 \ln(T_F/T)$ (or $(1/\tau) \sim \varepsilon^2 \ln(\varepsilon_F/\varepsilon)$ at zero temperature) showing no indication of the slow modes [34–37]. This is so because the lifetimes evaluated by the self-energy method are dominated by the fastest decay pathway, with the slow pathways due to long-lived modes providing a subleading contribution to the decay rates. A different scheme is therefore required for treating the slow and fast modes on equal footing.

Here we consider a simple model in which different harmonics of particle momentum distribution $\delta f_{\mathbf{p}} = \sum_m \delta f_m e^{im\theta}$, with the angle θ parametrizing the Fermi surface, relax at different rates. Microscopic analysis [33] predicts that (with log accuracy) the even-m harmonics relax at a constant rate $\gamma \sim T^2/T_F$, whereas the odd-m rates behave as $\gamma' m^p$ the exponent $p = 4$ and with $\gamma' \ll \gamma$:

$$\gamma_{m\,\text{even}} = \gamma(1 - \delta_{m,0}), \qquad \gamma_{m\,\text{odd}} = \gamma' m^p (1 - \delta_{m,\pm1}). \tag{3}$$

Zero values for $\gamma_{m=0,\pm1}$ reflect particle number and momentum conservation.

Below, we consider values $p = 4$ and 2, which describe different regimes of interest. The intrinsic relaxation mechanism due to ee collisions predicts the odd-m relaxation with $p = 4$ [33]. The case $p = 2$ is considered for illustration as well as having in mind that, in real systems, the very long lifetimes due to intrinsic effects can be overwhelmed by various extrinsic effects. For instance, relaxation due to small-angle scattering by a smooth disorder potential leads to conventional angular diffusion described by $p = 2$. The intrinsic m^4 scaling of the odd-m rates corresponds to angular superdiffusion [20], with a small γ', Eq. (2), taking on a role of the angular diffusion coefficient [see Eqs. (9) and (10)].

It might seem surprising that the modes with high m values could impact transport properties, since particle density and current—the two quantities usually probed in experiments—are described by $m = 0, \pm1$ harmonics. The significance of the high-m modes can be understood on

very general grounds in terms of the fluctuation-dissipation theorem, which mandates strong fluctuations for slowly relaxing degrees of freedom. Strong fluctuations, in turn, translate into enhanced scattering for other degrees of freedom, provided those are coupled to the slow degrees of freedom.

To clarify in a more quantitative way why different slow modes are coupled, we consider the transport equation, linearized near the $\mathbf{p}$-isotropic equilibrium state:

$$(\partial_t + \mathbf{v}\nabla - I_{ee})\delta f_{\mathbf{p}}(t, \mathbf{x}) = 0. \tag{4}$$

Couplings between different angular harmonics arise from the $\mathbf{v}\nabla$ term. To elucidate these couplings, we transform Eq. (4) to the δf_m basis, $\delta f_{\mathbf{p}} = \sum_m \delta f_m e^{im\theta}$. For plane-wave modes $\delta f_{\mathbf{p}}(t, \mathbf{x}) \sim e^{i\mathbf{k}\mathbf{x} - i\omega t}$, in the δf_m basis Eq. (4) takes the form of a 1D tight-binding model in which the eigenvalues of I_{ee} and $ikv/2$ represent the on-site potential and nearest-neighbor hopping amplitudes:

$$(\gamma_m - i\omega)\delta f_m = \frac{ikv}{2}\delta f_{m+1} + \frac{ikv}{2}\delta f_{m-1} \tag{5}$$

(without loss of generality we choose $\mathbf{k}\|x$). The hopping terms in Eq. (5) arise since $\cos\theta f(\theta)$ Fourier transforms to $\frac{1}{2}f_{m+1} + \frac{1}{2}f_{m-1}$. It is instructive to consider γ_m values that vanish on every other site, as in Eq. (3) in the limit $\gamma'/\gamma \to 0$. In this case, one can construct a nondecaying ($\omega = 0$) Bloch eigenstate described by δf_m vanishing on all the decaying sites with $\gamma_m \neq 0$ but nonzero on the non-decaying sites where $\gamma_m = 0$; namely,

$$\delta f_{m=2s+1} = (-1)^s, \qquad \delta f_{m=2s} = 0. \tag{6}$$

Equation (6) represents *a dark eigenstate* which is infinitely long-lived. Furthermore, the system hosts an entire band of long-lived near-dark states, with the lifetimes diverging in proximity of the dark state. Since these states have non-zero overlaps with the $m = \pm1$ harmonics that govern electric current, slow decay translates—by the fluctuation-dissipation theorem—into an enhancement of current fluctuations and higher conductivity. The latter, in turn, means reduced dissipation and lower viscosity.

The essential physics here resembles the slow-mode relaxation mechanism by Mandelshtam and Leontovich, and Debye, with the $m > 2$ harmonics playing the role of bath variables (see, e.g., Ref. [38], and references therein). Since mode coupling in Eq. (5) is proportional to kv, the impact of soft modes with high m is stronger at larger k. This can be seen as an underlying reason for transport coefficients such as conductivity and viscosity becoming scale dependent.

Turning to evaluating transport coefficients, we consider flows induced by an in-plane electric field varying as $\mathbf{E}(\mathbf{x}) = \mathbf{E}_{\mathbf{k}} \cos \mathbf{k}x$. Small deviations from equilibrium are described by a linearized kinetic equation,

$$(\partial_t + \mathbf{v}\nabla_{\mathbf{x}} - I_{ee})\delta f_{\mathbf{p}}(t,\mathbf{x}) = -e\mathbf{E}(\mathbf{x})\nabla_{\mathbf{p}}f_{\mathbf{p}}^{(0)}, \quad (7)$$

where $f_{\mathbf{p}}^{(0)}$ is the equilibrium distribution. The perturbed distribution $\delta f_{\mathbf{p}}$ is nonzero near the Fermi surface. Below, we will focus on the shear flows, described by $\mathbf{E}_{\mathbf{k}} \perp \mathbf{k}$.

Since the even and odd parts of the distribution $\delta f_{\mathbf{p}}(t,\mathbf{x})$ relax at very different rates, we employ an adiabatic approximation in order to "integrate out" the even-parity part and derive a closed-form equation for the odd-parity part. We first note that the only term in Eq. (7) that alters parity, $\mathbf{v}\nabla_{\mathbf{x}}$, transforms functions of odd parity to those of even parity, and vice versa. We can therefore decompose the distribution into a sum of an odd and an even contribution, $\delta f_{\mathbf{p}} = \delta f_{\mathbf{p}}^+ + \delta f_{\mathbf{p}}^-$, and write a system of coupled equations for these quantities:

$$(\partial_t - I_+)\delta f_{\mathbf{p}}^+(t,\mathbf{x}) + \mathbf{v}\nabla_{\mathbf{x}}\delta f_{\mathbf{p}}^-(t,\mathbf{x}) = 0,$$
$$(\partial_t - I_-)\delta f_{\mathbf{p}}^-(t,\mathbf{x}) + \mathbf{v}\nabla_{\mathbf{x}}\delta f_{\mathbf{p}}^+(t,\mathbf{x}) = -e\mathbf{E}(\mathbf{x})\nabla_{\mathbf{p}}f_{\mathbf{p}}^{(0)},$$
$$(8)$$

where $I_{\pm}$ denote the even-m and odd-m parts of I_{ee}. Since $I_+ = -\gamma$, the first equation yields a relation $\delta f_{\mathbf{p}}^+(t,\mathbf{x}) = -(1/\gamma)\mathbf{v}\nabla_{\mathbf{x}}\delta f_{\mathbf{p}}^-(t,\mathbf{x})$, valid at low frequencies $\omega \ll \gamma$, i.e., at the length scales $r \gg l_{ee}$. Plugging it in the second equation and interpreting m^p in I_- as the angle diffusion operator,

$$I_- = \sum_{m\,\text{odd}} -\gamma_m |m\rangle\langle m| \approx -\gamma'(i\partial_\theta)^p, \quad (9)$$

yields a closed-form relation for $\delta f_{\mathbf{p}}^-$. This relation will serve as a master equation for the new transport regime:

$$[\partial_t - D(\hat{\mathbf{v}}\nabla_{\mathbf{x}})^2 + \gamma'(i\partial_\theta)^p]\delta f_{\mathbf{p}}^-(t,\mathbf{x}) = -e\mathbf{E}(\mathbf{x})\nabla_{\mathbf{p}}f_{\mathbf{p}}^{(0)},$$
$$(10)$$

where we defined $D = v^2/\gamma$. Equation (10) describes "tomographic dynamics": fast one-dimensional spatial diffusion along the unchanging direction of velocity $\mathbf{v}$ accompanied by a slow angle diffusion that gradually randomizes the orientation of $\mathbf{v}$.

In the above derivation we ignored the $m = 0$ zero mode of I_+ since particle density remains unperturbed in the shear flows created by transverse fields $\mathbf{E}_{\mathbf{k}} \perp \mathbf{k}$. An extension of Eq. (10) accounting for this mode will be discussed elsewhere. Zero modes of I_- with $m = \pm 1$ can be accounted for by replacing in Eqs. (9) and (10) $\partial_\theta^2 \to \partial_\theta^2 - 1$. However, this change only matters in the long-wavelength hydrodynamic regime, at $r \gtrsim \xi$, and does not impact the behavior in the tomographic regime, Eq. (1). We therefore suppress such terms for the time being.

A perturbed momentum distribution can be obtained by inverting the transport operator in Eq. (10). Passing to

Fourier representation, $\delta f_{\mathbf{p}}(t,\mathbf{x}) = \delta f_{\mathbf{p}}e^{-i\omega t+i\mathbf{k}\mathbf{x}}$, we write a formal operator solution of Eq. (10) as

$$\delta f_{\mathbf{p}} = -\frac{1}{\hat{L} - i\omega}e\mathbf{E}\nabla_{\mathbf{p}}f_{\mathbf{p}}^{(0)}, \qquad \hat{L} = D(\hat{\mathbf{v}}\mathbf{k})^2 + \gamma'(i\partial_\theta)^p.$$
$$(11)$$

Writing $\mathbf{E}\nabla_{\mathbf{p}}f_{\mathbf{p}}^{(0)} = \mathbf{E}\mathbf{v}(\partial f_{\mathbf{p}}^{(0)}/\partial\varepsilon)$ and noting that $-(\partial f_{\mathbf{p}}^{(0)}/\partial\varepsilon) = \beta f_{\mathbf{p}}^{(0)}(1 - f_{\mathbf{p}}^{(0)}) \approx \delta(\varepsilon - \mu)$ confirms that the resulting perturbation indeed peaks at the Fermi level. Shear flows arise when $\mathbf{E}_{\mathbf{k}} = \int d^2x e^{-i\mathbf{k}\mathbf{x}}\mathbf{E}(\mathbf{x})$ is transverse to $\mathbf{k}$; without loss of generality here we take $\mathbf{E}_{\mathbf{k}}\|\hat{\mathbf{y}}, \mathbf{k}\|\hat{\mathbf{x}}$.

The transport operator $\hat{L}$ acts on the Fermi surface parametrized by the angle θ; it is a sum of two non-commuting contributions, $(\hat{\mathbf{v}}\mathbf{k})^2 = k^2\cos^2\theta$ and $(i\partial_\theta)^p$. One is diagonal in the θ representation, the other is diagonal in the δf_m representation. Diagonalizing $\hat{L}$, therefore, represents a nontrivial task. Assuming that the eigenfunctions and eigenvalues of $\hat{L}$, defined by $\hat{L}\psi_n(\theta) = \lambda_n\psi_n(\theta)$, are known, we can write the inverse as

$$\left\langle\theta\left|\frac{1}{\hat{L} - i\omega}\right|\theta'\right\rangle = \sum_n\frac{\bar{\psi}_n(\theta)\psi_n(\theta')}{\lambda_n - i\omega}. \quad (12)$$

Using Eq. (12) we proceed to evaluate current $j_{y,\mathbf{k}} = ev\nu_0\oint(d\theta/2\pi)\sin\theta\delta f(\theta)$, where ν_0 is the density of states at ε_F. Plugging in the angle dependence $\mathbf{E}\mathbf{v} = Ev\sin\theta$ gives

$$\mathbf{j}_{\mathbf{k}} = e^2v^2\nu_0\mathbf{E}_{\mathbf{k}}\oint\frac{d\theta}{2\pi}\oint\frac{d\theta'}{2\pi}\sin\theta\left\langle\theta\left|\frac{1}{\hat{L} - i\omega}\right|\theta'\right\rangle\sin\theta'.$$
$$(13)$$

We can rewrite this relation as $\mathbf{j}_{\mathbf{k}} = \sigma(k,\omega)\mathbf{E}_{\mathbf{k}}$ by introducing a scale-dependent conductivity:

$$\sigma(k,\omega) = e^2v^2\nu_0\sum_n\frac{|\langle\sin\theta|\psi_n(\theta)\rangle|^2}{\lambda_n - i\omega}. \quad (14)$$

The matrix elements $\langle\sin\theta|\psi_n(\theta)\rangle$ quickly decrease with n, allowing us to estimate the sum in Eq. (14) by retaining only the $n = 0$ term. The lowest eigenvalue can be found by the variational method as

$$\lambda_0 = \min\langle\psi|\hat{L}|\psi\rangle \sim \min\left(Dk^2\delta\theta^2 + \frac{\gamma'}{\delta\theta^p}\right). \quad (15)$$

Here the trial state is normalized, $\langle\psi|\psi\rangle = 1$, and is localized within the region of width $\delta\theta$ near the minima of $\cos^2\theta$, i.e., around $\theta = \pm\pi/2$. The estimate in Eq. (15) gives the width $\delta\theta \sim (\gamma'/Dk^2)^{1/(2+p)}$ and the value

$$\lambda_0 \sim Dk^2\left(\frac{\gamma'}{Dk^2}\right)^{2/(2+p)}. \quad (16)$$

Plugging these values in Eq. (14) and setting $\omega = 0$ gives a scale-dependent dc conductivity:

$$\sigma(k) \sim \frac{e^2 v^2 \nu_0}{Dk^2} \left(\frac{Dk^2}{\gamma'}\right)^{1/(2+p)} \sim k^{-2+2/(2+p)}. \quad (17)$$

Our variational estimate is valid provided $\delta\theta \ll 1$, which translates into the condition $k > (\gamma'/D)^{1/2} = 1/\xi$ identical to the upper limit in Eq. (1) that marks the tomographic-hydrodynamic crossover.

Viscosity scale dependence can now be inferred by comparing Eq. (17) to the conductivity $\sigma(k) = (n^2 e^2/\eta k^2)$ obtained from the Stokes equation $-\eta\nabla^2 \mathbf{v} = ne\mathbf{E}$, giving

$$\eta(k) \sim k^{-2/(2+p)}. \quad (18)$$

Equation (18) predicts viscosity growing versus length scale, in agreement with the qualitative picture discussed above. The scaling exponents are $-1/3$ and $-1/2$ for the cases $p = 4$ and 2, respectively.

These results are valid for wave numbers in the range $l_{ee}^{-1} > k > \xi^{-1}$; see Eq. (1). Larger values $k > l_{ee}^{-1}$ correspond to ballistic free-particle transport; smaller values $k < \xi^{-1}$ correspond to hydrodynamic transport. At $k\xi \sim 1$ our k-dependent viscosity values $\nu(k)$ match the standard hydrodynamic value $\eta_{\text{hydro}} = nmv^2/4\gamma$. At shorter length scales, $k\xi > 1$, the viscosity is reduced compared to η_{hydro} by a factor $(k\xi)^{2/(2+p)}$. The reduction in η is maximal at $k \sim l_{ee}^{-1}$, where $\eta(k)/\eta_{\text{hydro}} \sim (\gamma'/\gamma)^{1/(2+p)}$. This scale dependence implies that, somewhat unexpectedly, the system behavior, which is liquidlike at small distances, becomes more gaseous at larger distances.

Next, we demonstrate that scale dependence of σ and η manifests itself in a characteristic current distribution across sample cross section, which is distinct from the familiar parabolic distribution for conventional viscous flows. We analyze flow in a strip $0 < x < w$, $-\infty < y < \infty$ with momentum relaxation at the boundaries $x = 0$, w. To simplify the geometry, we consider an auxiliary problem in an infinite (x, y) plane equipped with an array of lines, spaced by w, where current relaxation may occur. Current induced by an E field, which is parallel to the lines, is given by

$$j(x) = \int dx' \sigma(x - x') \left[E - \alpha \sum_i j(x_i)\delta(x - x_i)\right], \quad (19)$$

with $x_i = wi$. Here, α is a parameter that is a property of the lines, representing strip boundary, and $\sigma(x - x') = \int (dk/2\pi)e^{ik(x-x')}\sigma(k)$. The limit $\alpha \to \infty$ is taken at the end of the calculation to mimic diffuse boundary conditions.

Current distribution for this problem can be obtained by the Fourier method, by writing

$$j(x) = \sum_n j_n e^{k_n x}, \qquad k_n = \frac{2\pi}{w}n, \qquad n = 0, \pm 1, \pm 2, \dots. \quad (20)$$

Plugging this expression in Eq. (19) and Fourier transforming, we have a system of coupled equations for j_n:

$$\rho_n j_n = E\delta_{n,0} - \tilde{\alpha}\sum_{n'} j_{n'}, \qquad \rho_n = \frac{1}{\sigma(k_n)}, \quad (21)$$

where we defined $\tilde{\alpha} = \alpha/w$. These equations can be solved by separating the $n = 0$ and $n \neq 0$ harmonics:

$$(\rho_0 + \tilde{\alpha})j_0 = E - \tilde{\alpha}\sum{}' j_{n'}, \quad j_n = \sigma(k_n)\left(-\tilde{\alpha}j_0 - \tilde{\alpha}\sum{}' j_{n'}\right). \quad (22)$$

where we introduced a shorthand notation $\sum' = \sum_{n' \neq 0}$. Taking a sum over all $n \neq 0$ harmonics yields a relation

$$(1 + \tilde{\alpha}G)\sum{}' j_n = -\tilde{\alpha}G j_0, G = \sum{}' \sigma(k_n). \quad (23)$$

Expressing $\sum' j_{m'}$ and combining with the first equation in Eq. (22), we obtain

$$\left(\rho_0 + \frac{\tilde{\alpha}}{1 + \tilde{\alpha}G}\right)j_0 = E. \quad (24)$$

For the case when there are no Ohmic losses, $\rho_0 = 0$, and in the limit $\alpha \to \infty$, this relation simplifies to

$$j_0 = E\sum{}' \sigma(k_n). \quad (25)$$

The distribution of current within the strip then is

$$j(x) = j_0\left(1 - \frac{\sum' \sigma(k_n)e^{ik_n x}}{\sum' \sigma(k_n)}\right). \quad (26)$$

For conventional scale-independent viscosity, substituting $\sigma(k) = (1/\nu k^2)$, this expression, after a little algebra, gives the familiar parabolic profile $j(x) \sim x(w - x)$. For scale-dependent viscosity $\nu(k) \sim k^{-2/(2+p)}$ it yields a distribution closely resembling the fractional-power profile:

$$j(0 < x < w) \sim x^{2/(2+p)}(w - x)^{2/(2+p)}. \quad (27)$$

The resulting current profiles are illustrated in Fig. 2 for several cases of interest. We see that the k dependence of σ and η has a strong impact on the current profile, providing a directly measurable signature of the tomographic regime.

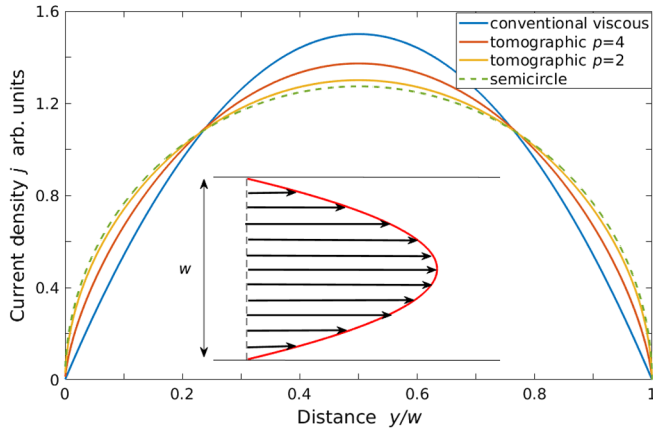This analysis points to several other interesting aspects of tomographic dynamics. First, the system conductance

FIG. 2.   Current density in a long strip of width w induced by a uniform dc electric field, Eq. (26). Inset: Flow schematic. The flow profile is different for the conventional viscous and tomographic regimes, showing signatures that depend on the angular relaxation dynamics type, parametrized by $p = 4$ and 2. A semicircle is shown as a guide to the eye.

dependence versus strip width can be obtained by noting that the sum in Eq. (25) converges rapidly, and is well approximated by the first term, $m = 1$. This predicts scaling for the conductance of the form

$$G(w) \sim w^{3-2/(2+p)}, \tag{28}$$

a dependence that *lies in between* the seminal Poisseuille-Gurzhi scaling w^3 for the conventional viscous regime [1] and w^2 scaling for the ballistic transport regime [39].

Second, velocities of current-carrying electrons are tightly collimated along the strip axis, spanning angles in the range estimated above, $\delta\theta_{k_1} = (\xi k_1)^{-2/(2+p)} \ll 1$. This is in stark contrast to conventional viscous flows, where velocities are nearly isotropic. Strong velocity collimation tunable by the *ee* collision rate is a surprising behavior, which, along with the peculiar fractional-power conductance scaling, provides a clear signature of the tomographic regime.

[1] R. N. Gurzhi, Hydrodynamic effects in solids at low temperature, Usp. Fiz. Nauk **94**, 689 (1968) [Sov. Phys. Usp. **11**, 255 (1968)].

[2] E. M. Lifshitz and L. P. Pitaevskii, *Physical Kinetics* (Pergamon Press, New York, 1981).

[3] M. J. M. de Jong and L. W. Molenkamp, Hydrodynamic electron flow in high-mobility wires, Phys. Rev. B **51**, 13389 (1995).

[4] R. Jaggi, Electron-fluid model for the dc size effect, J. Appl. Phys. **69**, 816 (1991).

[5] K. Damle and S. Sachdev, Nonzero-temperature transport near quantum critical points, Phys. Rev. B **56**, 8714 (1997).

[6] D. E. Sheehy and J. Schmalian, Quantum Critical Scaling in Graphene, Phys. Rev. Lett. **99**, 226803 (2007).

[7] L. Fritz, J. Schmalian, M. Müller, and S. Sachdev, Quantum critical transport in clean graphene, Phys. Rev. B **78**, 085416 (2008).

[8] A. V. Andreev, S. A. Kivelson, and B. Spivak, Hydrodynamic Description of Transport in Strongly Correlated Electron Systems, Phys. Rev. Lett. **106**, 256804 (2011).

[9] D. Forcella, J. Zaanen, D. Valentinis, and D. van der Marel, Electromagnetic properties of viscous charged fluids, Phys. Rev. B **90**, 035143 (2014).

[10] A. Tomadin, G. Vignale, and M. Polini, Corbino Disk Viscometer for 2D Quantum Electron Liquids, Phys. Rev. Lett. **113**, 235901 (2014).

[11] B. N. Narozhny, I. V. Gornyi, M. Titov, M. Schütt, and A. D. Mirlin, Hydrodynamics in graphene: Linear-response transport, Phys. Rev. B **91**, 035414 (2015).

[12] A. Principi, G. Vignale, M. Carrega, and M. Polini, Bulk and shear viscosities of the 2D electron liquid in a doped graphene sheet, Phys. Rev. B **93**, 125410 (2016).

[13] A. Lucas, R. A. Davison, and S. Sachdev, Hydrodynamic theory of thermoelectric transport and negative magneto-resistance in Weyl semimetals, Proc. Natl. Acad. Sci. U.S.A. **113**, 9463 (2016).

[14] P. S. Alekseev, Negative Magnetoresistance in Viscous Flow of Two-Dimensional Electrons, Phys. Rev. Lett. **117**, 166601 (2016).

[15] B. N. Narozhny, I. V. Gornyi, A. D. Mirlin, and J. Schmalian, Hydrodynamic approach to electronic transport in graphene, Ann. Phys. (Berlin) **529**, 1700043 (2017).

[16] T. Scaffidi, N. Nandi, B. Schmidt, A. P. Mackenzie, and J. E. Moore, Hydrodynamic Electron Flow and Hall Viscosity, Phys. Rev. Lett. **118**, 226601 (2017).

[17] O. Kashuba, B. Trauzettel, and L. W. Molenkamp, Relativistic Gurzhi effect in channels of Dirac materials, Phys. Rev. B **97**, 205129 (2018).

[18] A. Lucas and K. C. Fong, Hydrodynamics of electrons in graphene, J. Phys. Condens. Matter **30**, 053001 (2018).

[19] Y. H. Ho Derek, I. Yudhistira, N. Chakraborty, and S. Adam, Theoretical determination of hydrodynamic window in monolayer and bilayer graphene from scattering rates, Phys. Rev. B **97**, 121404(R) (2018).

[20] P. J. Ledwith, H. Guo, L. Levitov, Angular dynamics and directional memory in two-dimensional electron fluids, arXiv:1708.01915.

[21] L. Levitov and G. Falkovich, Electron viscosity, current vortices and negative nonlocal resistance in graphene, Nat. Phys. **12**, 672 (2016).

[22] H. Guo, E. Ilseven, G. Falkovich, and L. Levitov, Higher-than-ballistic conduction of viscous electron flows, Proc. Natl. Acad. Sci. **114,** 3068 (2017).

[23] J. Crossno *et al.*, Observation of the Dirac fluid and the breakdown of the Wiedemann-Franz law in graphene, Science **351,** 1058 (2016).

[24] D. A. Bandurin *et al.*, Negative local resistance caused by viscous electron backflow in graphene, Science **351,** 1055 (2016).

[25] R. Krishna Kumar *et al.*, Superballistic flow of viscous electron fluid through graphene constrictions, Nat. Phys. **13,** 1182 (2017).

[26] D. A. Bandurin, A. V. Shytov, L. S. Levitov, R. Krishna Kumar, A. I. Berdyugin, M. Ben Shalom, I. V. Grigorieva, A. K. Geim, and G. Falkovich, Fluidity onset in graphene, Nat. Commun. **9,** 4533 (2018).

[27] A. I. Berdyugin *et al.*, Measuring Hall viscosity of graphene's electron fluid, Science **364,** 162 (2019).

[28] P. J. W. Moll, P. Kushwaha, N. Nandi, B. Schmidt, and A. P. Mackenzie, Evidence for hydrodynamic electron flow in $PdCoO_2$, Science **351,** 1061 (2016).

[29] B. A. Braem, F. M. D. Pellegrino, A. Principi, M. Röösli, C. Gold, S. Hennel, J. V. Koski, M. Berl, W. Dietsche, W. Wegscheider, M. Polini, T. Ihn, and K. Ensslin, Scanning gate microscopy in a viscous electron fluid Phys. Rev. B **98,** 241304(R) (2018).

[30] B. Laikhtman, Electron-electron angular relaxation in a two-dimensional electron gas, Phys. Rev. B **45,** 1259 (1992).

[31] R. N. Gurzhi, A. N. Kalinenko, and A. I. Kopeliovich Electron-Electron Collisions and a New Hydrodynamic Effect in Two-Dimensional Electron Gas, Phys. Rev. Lett. **74,** 3872 (1995).

[32] H. Buhmann and L. W. Molenkamp, 1D diffusion: A novel transport regime in narrow 2DEG channels, Physica (Amsterdam) **12E,** 715 (2002).

[33] P. J. Ledwith, H. Guo, and L. Levitov, The hierarchy of excitation lifetimes in two-dimensional Fermi gases, Ann. Phys. (Amsterdam) https://doi.org/10.1016/j.aop.2019.167913 (2019).

[34] A. V. Chaplik, Energy spectrum and electron scattering processes in inversion layers, Zh. Eksp. Teor. Fiz. **60,** 1845 (1971) [Sov. Phys. JETP **33,** 997 (1971)].

[35] C. Hodges, H. Smith, and J. W. Wilkins, Effect of Fermi surface geometry on electron-electron scattering, Phys. Rev. B **4,** 302 (1971).

[36] P. Bloom, Two-dimensional Fermi gas, Phys. Rev. B **12,** 125 (1975).

[37] G. F. Giuliani and J. J. Quinn, Lifetime of a quasiparticle in a two-dimensional electron gas, Phys. Rev. B **26,** 4421 (1982).

[38] A. P. Levanyuk, Contribution to a phenomenological theory of sound absorption near second-order phase transition points, Sov. Phys. JETP **22,** 901 (1966).

[39] C. W. J. Beenakker and H. van Houten, Quantum transport in semiconductor nanostructures, Solid State Phys. **44,** 1 (1991).